Teleconnections between Rainfall in Equatorial Africa and Tropical Sea Surface Temperatures: A Focus on Western Uganda

JEREMY E. DIEM,[a] JONATHAN D. SALERNO,[b] MICHAEL W. PALACE,[c] KAREN BAILEY,[d] AND JOEL HARTTER[d]

[a] *Georgia State University, Atlanta, Georgia*
[b] *Colorado State University, Fort Collins, Colorado*
[c] *University of New Hampshire, Durham, New Hampshire*
[d] *University of Colorado Boulder, Boulder, Colorado*

(Manuscript received 29 March 2021, in final form 10 June 2021)

ABSTRACT: Substantial research on the teleconnections between rainfall and sea surface temperatures (SSTs) has been conducted across equatorial Africa as a whole, but currently no focused examination exists for western Uganda, a rainfall transition zone between eastern equatorial Africa (EEA) and central equatorial Africa (CEA). This study examines correlations between satellite-based rainfall totals in western Uganda and SSTs—and associated indices—across the tropics over 1983–2019. It is found that rainfall throughout western Uganda is teleconnected to SSTs in all tropical oceans but is connected much more strongly to SSTs in the Indian and Pacific Oceans than in the Atlantic Ocean. Increased Indian Ocean SSTs during boreal winter, spring, and autumn and a pattern similar to a positive Indian Ocean dipole during boreal summer are associated with increased rainfall in western Uganda. The most spatially complex teleconnections in western Uganda occur during September–December, with northwestern Uganda being similar to EEA during this period and southwestern Uganda being similar to CEA. During boreal autumn and winter, northwestern Uganda has increased rainfall associated with SST patterns resembling a positive Indian Ocean dipole or El Niño. Southwestern Uganda does not have those teleconnections; in fact, increased rainfall there tends to be more associated with La Niña–like SST patterns. Tropical Atlantic Ocean SSTs also appear to influence rainfall in southwestern Uganda in boreal winter as well as in boreal summer. Overall, western Uganda is a heterogeneous region with respect to rainfall–SST teleconnections; therefore, southwestern Uganda and northwestern Uganda require separate analyses and forecasts, especially during boreal autumn and winter.

SIGNIFICANCE STATEMENT: Seasonal rainfall greatly impacts the millions of rural households practicing rain-fed agriculture across equatorial Africa; therefore, understanding the relationship between rainfall and tropical sea surface temperatures (SSTs) can benefit smallholder farmers and other stakeholders. This study examines over the 1983–2019 period the relationships between SSTs and monthly and seasonal rainfall totals in western Uganda. During Northern Hemisphere (boreal) spring and summer, increased SSTs in the Indian Ocean along with La Niña–like SST patterns are generally associated with increased rainfall for the entire region. Rainfall–SST relationships have substantial spatial variability during boreal autumn and winter: only northwestern Uganda has increased rainfall strongly associated with the positive Indian Ocean dipole and El Niño–like SST patterns. These findings have implications for the region-specific forecasts provided to farmers.

KEYWORDS: Africa; Teleconnections; Rainfall; ENSO; Seasonal variability

1. Introduction

People throughout equatorial Africa are highly vulnerable to the impacts of rainfall variability. This region is home to millions of rural households practicing rain-fed agriculture, and their food security depends on the timing and amount of rainfall within rainy seasons (Cooper et al. 2008; Zougmoré et al. 2018). For instance, based on observation and predictions of seasonal rainfall patterns, farmers select crop types and varieties, choose where and when to plant, and apply a suite of adaptive management practices (Wilkie et al. 1999; Crane et al. 2011; Salerno et al. 2019). Drought can severely reduce food security in countries such as Kenya and Somalia (Nicholson 2014). Excessive rainfall also is detrimental to agriculture since it increases the likelihood of crop loss due to rot and pests (Farrow et al. 2011; Okonya et al. 2013). Heavy rainfall can exacerbate soil erosion, with the 1997/98 rainfall in Kenya associated with an El Niño event a prime example (Ngecu and Mathu 1999). Moreover, negative impacts of adverse rainfall conditions extend beyond farming; for example, excessive rainfall can exacerbate the incidence of disease such as malaria (Ssempiira et al. 2018).

Rainfall within equatorial Africa is far from uniform. Much of the western portion has the Congo rain forest with annual rainfall exceeding 1500 mm (Todd and Washington 2004), while some places in the far eastern portion have arid climates with annual rainfall less than 600 mm (Herrmann and Mohr 2011) (Fig. 1a). Two adjacent areas for which climate has been studied at the regional scale are eastern equatorial Africa (EEA) and central equatorial Africa (CEA). These two regions differ not just in rainfall quantity but also in intra-annual characteristics of rainfall: EEA has a biannual rainfall regime (i.e., two rainy seasons), with more rainfall occurring during

Corresponding author: Jeremy E. Diem, jdiem@gsu.edu

DOI: 10.1175/JAMC-D-21-0057.1

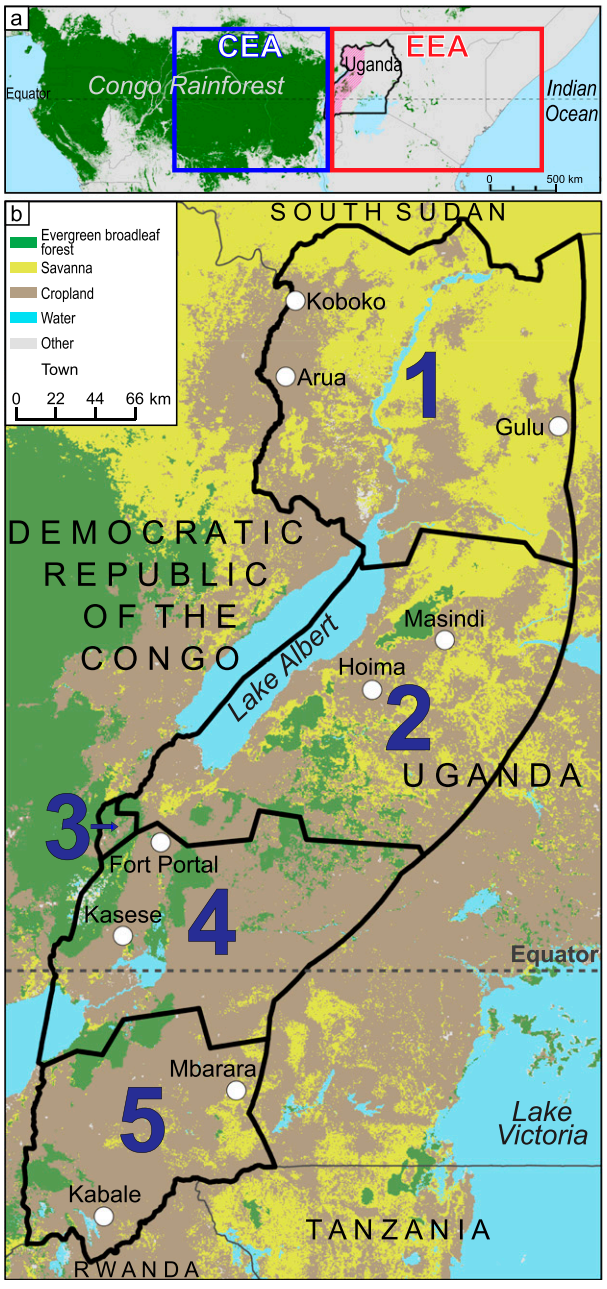

FIG. 1. (a) Location of the western Uganda study area, a zone within 160 km of the Congo basin (Diem et al. 2019a), with respect to the Congo rain forest, central equatorial Africa (CEA), and eastern equatorial Africa (EEA). (b) The five rainfall regions, the major towns, and the dominant land-cover types in western Uganda. Land-cover information is derived from the MODIS land-cover-type product (MCD12Q1).

boreal spring (i.e., the long rains) than during boreal autumn (i.e., the short rains) (Camberlin et al. 2009; Liebmann et al. 2012), whereas CEA has a biannual regime but with more rainfall in boreal autumn than in boreal spring (Creese and Washington 2018).

Circulation in EEA and CEA is complex, with both zonal and meridional circulations present. The Hadley circulation is composed of meridional overturning cells and is well structured over the oceans, with trade winds from both hemispheres converging at the intertropical convergence zone (ITCZ), which on average is located in the Northern Hemisphere (Webster 2004; Marshall et al. 2014). Over the African continent, the ITCZ is better characterized as the tropical rain belt since, for the most part, trade winds do not exist over Africa (Nicholson 2018). The rain belt is oriented east to west, migrates latitudinally, and experiences much more movement over EEA than over CEA (Nicholson 2018). The Walker circulation is composed of zonal overturning cells across the tropics, with upward motion typically present over the Congo basin (Cook and Vizy 2016) and downward motion typically present over the western Indian Ocean and far eastern EEA (Lau and Yang 2015; King et al. 2020). Associated with the tropical rain belt is the Congo air boundary, which is a confluence zone oriented southwest to northeast, where westerly air from the Congo basin meets easterly air from the Indian Ocean (Nicholson 2000; Levin et al. 2009; Costa et al. 2014; Dezfuli 2017).

El Niño–Southern Oscillation (ENSO) and the Indian Ocean dipole (IOD) are oscillations of tropical sea surface temperatures (SSTs) that impact the Walker circulation—and ultimately rainfall—over EEA and CEA. Surface westerlies are typical across the Indian Ocean (Hastenrath and Polzin 2004), and those westerlies prevail across the Indian Ocean during a La Niña event (Lau and Yang 2015). During an El Niño event, there is a weakening of the Indian Ocean Walker cell and thus a shift to easterly winds across the Indian Ocean (Camberlin et al. 2001; Lau and Yang 2015). High SSTs in the western Indian Ocean and low SSTs in the southeastern Indian Ocean represent positive IOD events, and low SSTs in the western Indian Ocean and high SSTs in the southeastern Indian Ocean represent negative IOD events (Saji et al. 1999). These events are referred to herein as positive IOD (pIOD) and negative IOD (nIOD). A pIOD event forces anomalous southeasterly trade winds that increase moisture supply into EEA from the Indian Ocean (Black et al. 2003; Liebmann et al. 2014). pIOD events often co-occur with El Niño events (Schott et al. 2009), with El Niño possibly predisposing the Indian Ocean coupled system to a pIOD event (Black et al. 2003).

a. Rainfall teleconnections with SSTs

1) INDIAN OCEAN

Increased SSTs in the Indian Ocean, particularly in the western portion, tend to be teleconnected (i.e., connected across a large geographical scale) to increased rainfall in both EEA and CEA. There are nonexistent to weakly positive correlations between boreal spring rainfall in both EEA and CEA and Indian Ocean SSTs (Nicholson and Dezfuli 2013; Omondi et al. 2013; Lyon 2014; Vellinga and Milton 2018). The IOD becomes a factor in boreal summer and autumn in EEA: pIOD-like patterns are positively correlated with rainfall in southeastern Ethiopia during boreal summer (Dubache et al. 2019) and with rainfall throughout EEA during boreal autumn

(Black et al. 2003; Lyon 2014; Bahaga et al. 2015; Nicholson 2015; Wenhaji Ndomeni et al. 2018; Endris et al. 2019). Whereas rainfall in CEA is not strongly correlated with Indian Ocean SSTs in boreal summer (Creese and Washington 2016), there is increased rainfall in boreal autumn in far eastern CEA when the western Indian Ocean is warmer (Dezfuli and Nicholson 2013).

2) PACIFIC OCEAN

Wet boreal winters and autumns in EEA are teleconnected to El Niño–like SST patterns, wet boreal springs have relatively weak teleconnections to tropical Pacific Ocean SSTs, and wet boreal summers are teleconnected to La Niña–like SST patterns. While few studies focus on boreal winter, the season is likely wetter over the region during El Niño years and drier over the region during La Niña years (de Oliveira et al. 2018). There has been much more research on the teleconnections between ENSO and the "short rains" of boreal autumn, with the major findings that El Niño and La Niña lead to increased and decreased rainfall, respectively (Mutai and Ward 2000; Camberlin et al. 2001; Black et al. 2003; Schreck and Semazzi 2004; Lyon 2014; Wenhaji Ndomeni et al. 2018; Endris et al. 2019). In addition, EEA may receive increased rainfall only when El Niño occurs synchronously with a pIOD event (Black 2005; Behera et al. 2005; Bahaga et al. 2015; MacLeod et al. 2021). During boreal spring, there are weak negative correlations between rainfall and SSTs in the central and eastern equatorial Pacific Ocean (Camberlin et al. 2001; Camberlin and Philippon 2002; Endris et al. 2019). Weak positive correlations between rainfall and central equatorial Pacific Ocean SSTs also have been found for boreal spring (Lyon 2014). Strong negative correlations between rainfall and central and eastern equatorial Pacific Ocean SSTs exist during boreal summer (Camberlin et al. 2001; Segele et al. 2009; Berhane et al. 2014; Lyon 2014; Degefu et al. 2017; Gleixner et al. 2017; de Oliveira et al. 2018; Endris et al. 2019).

CEA generally has increased rainfall teleconnected to La Niña–like SST patterns (i.e., decreased rainfall and El Niño–like SST patterns). Rainfall is positively correlated with La Niña–like patterns during boreal winter (Balas et al. 2007), boreal spring (Camberlin et al. 2001; Nicholson and Dezfuli 2013), and boreal summer (Balas et al. 2007; Endris et al. 2019). Rainfall in the far eastern portion during boreal autumn, specifically October–December, appears to be positively correlated with El Niño–like SST patterns (Dezfuli and Nicholson 2013). However, pure El Niño events (i.e., with no connection to an IOD phase) are associated with decreased rainfall during September–November (Bahaga et al. 2015).

3) ATLANTIC OCEAN

Teleconnections between Atlantic Ocean SSTs and seasonal rainfall in EEA and CEA are not especially strong. Throughout most of EEA there are no significant correlations between rainfall and tropical Atlantic Ocean SSTs (Camberlin et al. 2001; Degefu et al. 2017). Boreal spring rainfall in CEA is positively (negatively) correlated with tropical south (north) Atlantic SSTs; the positive correlation also includes Gulf of Guinea SSTs (Nicholson and Dezfuli 2013). Warm SST anomalies in the southern tropical Atlantic Ocean are associated with wet (dry) boreal summers (winters) in CEA (Balas et al. 2007). There is likely no connection between Atlantic Ocean SSTs and CEA rainfall during boreal autumn (Creese and Washington 2018).

b. *Purpose and objectives of study*

Western Uganda is an important area to focus on for several reasons. First, since western Uganda is transitional between EEA and CEA with respect to rainfall (Monaghan et al. 2012; Diem et al. 2019a), detailed analyses of tropical SST teleconnections with rainfall in the region fills a critical gap in our understanding of the climate of equatorial Africa. Currently, only rough estimates of teleconnections have been deduced based on results from EEA and CEA studies. Second, millions of people (with some of the most concentrated and fastest growing human populations on the planet) depend on rainfed agriculture for livelihoods in western Uganda (Diem et al. 2017), and those smallholder farmers currently desire more accurate seasonal rainfall forecasts from the government (Osbahr et al. 2011; Roncoli et al. 2011) and might be becoming increasingly reliant on seasonal forecasts in the future (Roncoli et al. 2002). Rainfall–SST teleconnections play an important role in the forecasts the Uganda National Meteorological Authority (UNMA) produces for regions within Uganda: those forecasts are based largely on IOD and ENSO conditions (UNMA 2021). Third, western Uganda has likely had increasing rainfall trends in all seasons except for boreal winter (Diem et al. 2019a,b)—which makes it unique within equatorial Africa—and understanding rainfall–SST teleconnections will provide a foundation for future research that attempts to understand the wetting trend in the region.

The purpose of this research is to better understand how rainfall in western Uganda is teleconnected to tropical SSTs of the Indian, Pacific, and Atlantic Oceans. The study involves months in addition to seasons, because existing studies have used a variety of season definitions (e.g., September–November and October–November for boreal autumn) and—as Nicholson (2017) notes—there can be markedly different teleconnections among the months within a season. The objectives for this study are as follows: 1) to identify statistically significant teleconnections between seasonal and monthly rainfall and concurrent tropical SSTs and associated indices and 2) to examine the spatial complexity of the intra-annual variability in teleconnections.

2. Study area

Western Uganda has rainfall totals and seasonal rainfall variability that are transitional between EEA and CEA (Figs. 1 and 2). Diem et al. (2019b) divided western Uganda into five homogeneous rainfall regions that represented latitudinal zones as well as a western region, region 3, that is a small portion of lowland rain forest extending into the Congo basin. Annual rainfall totals for the five regions ranges from ~1100 to ~1400 mm (Fig. 2). These rainfall totals are higher than the mean for EEA (Nicholson 2017) but lower than the mean for CEA (Todd and Washington 2004). Region 1, the northernmost region, exists between 2° and 4°N latitude and has an annual rainfall regime, with the one long rainy season occurring from late March to mid-November. The rest of the regions

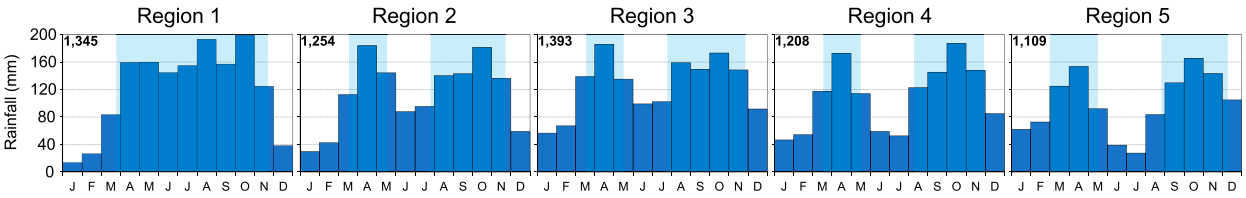

FIG. 2. Mean monthly rainfall totals over 1983–2019 for the five rainfall regions. Annual rainfall totals (mm) are shown in the upper-left corner of each panel. Approximate rainy-season periods are shown with light-blue shading. The mean of CHIRPS and TAMSAT data were used to estimate rainfall totals (see section 3 for a description of the satellite-based rainfall data). Rainy-season information is based on information in Fig. 2 in Diem et al. (2019b).

are much closer to the equator and have biannual rainfall regimes, with the first rainy season typically occurring from mid-March to mid-May and the second rainy season occurring from August through November. Region 5, the southernmost region, has slightly different rainy seasons than the other regions with a biannual regime: the first rains begin earlier (i.e., March 1) and the second rains start later (i.e., late August) and end later (i.e., early December). For the four regions with a biannual rainfall regime, the second rains are approximately 50 days longer (i.e., 116 vs 66 days) than the first rains. Consequently, in contrast to most parts of EEA, the first rains in western Uganda are called the "short rains" and second rains are called the "long rains" (Hartter et al. 2012; Diem et al. 2017).

3. Data and methods

Rainfall data consisted of satellite-based rainfall estimates from two rainfall products. Daily estimates for 1983–2019 from version 2 of Climate Hazards Group Infrared Precipitation with Station data (CHIRPS; Funk et al. 2015) and version 3 of Tropical Applications of Meteorology Using Satellite and Ground-Based Observations (TAMSAT; Maidment et al. 2017) were obtained from the International Research Institute for Climate and Society at Columbia University. For all analyses, the mean of the CHIRPS and TAMSAT values was used to decrease the impact of any errors in one of the products. CHIRPS and TAMSAT were selected because they share several important similarities: 1) they have strong temporal correlations with ground-measured rainfall in western Uganda (Diem et al. 2019a), 2) they extend back to at least 1983, and 3) they have relatively high spatial resolutions (i.e., 0.05° for CHIRPS and 0.0375° for TAMSAT). CHIRPS was serially complete, while TAMSAT was missing 5% of daily rainfall totals. For each of those 678 days with missing data, the mean value for the day of year was used as the predicted rainfall total.

Tropical-SST data included gridded SSTs and associated indices. Gridded SST data were extracted from the Optimal Interpolation SST Analysis, version 2 (OISSTV2) (Reynolds et al. 2002); the data were acquired from the National Oceanic and Atmospheric Administration (NOAA). The data have 1° spatial resolution. The Indian Ocean SST indices consisted of the western tropical Indian Ocean (WTIO) index, the southeastern tropical Indian Ocean (SETIO) index, and the dipole mode index (DMI). The DMI, the difference between the WTIO and SETIO indices, is an indicator of the Indian Ocean dipole (Saji et al. 1999). The Pacific Ocean indices consisted of the western Pacific (WP) index, the Niño-4 index, the Niño-3.4 index, the Niño-3 index, the Niño-1+2 index, and the Southern Oscillation index (SOI). The OISSTV2 data were used to calculate the WP index, which is the mean SST within 0°–10°N and 130°–150°W (Hoell and Funk 2013). The Atlantic Ocean SST indices consisted of the North Atlantic tropical (NAT) index, the South Atlantic tropical (SAT) index, and the tropical Atlantic meridional gradient (TAMG) index. The TAMG, the difference between the NAT and SAT indices, is an indicator of the meridional SST gradient in the tropical Atlantic Ocean and thus the north–south displacement of the Atlantic ITCZ (Chang et al. 1997; Mélice and Servain 2003). The spatial domains of the SST indices described above are shown on Fig. 3. All indices except for WP were acquired from NOAA.

Temporal correlations between rainfall and SSTs and associated indices were calculated from 1983 to 2019. The rainfall regions determined by Diem et al. (2019b) were used, and the mean of the CHIRPS and TAMSAT values was used as the rainfall total for each region. Correlations were calculated for each region–month combination and each region–season combination. The selected months corresponding to boreal winter, spring, summer, and autumn were December–

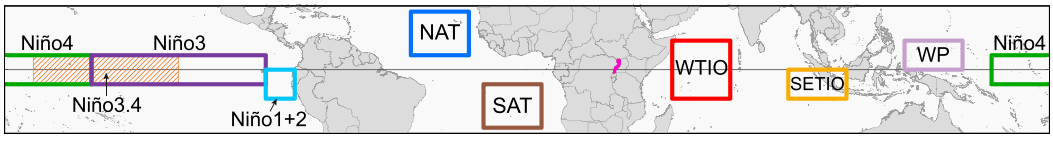

FIG. 3. Locations of the 10 regions from which tropical SST indices are calculated. Western Uganda is highlighted in color. In addition to the Niño indices in the central and eastern equatorial Pacific Ocean are the following: the North Atlantic Tropical (NAT) index, the South Atlantic Tropical (SAT) index, the Western Tropical Indian Ocean (WTIO) index, the Southeastern Tropical Indian Ocean (SETIO) index, and the Western Pacific (WP) index. The indices are described in section 3.

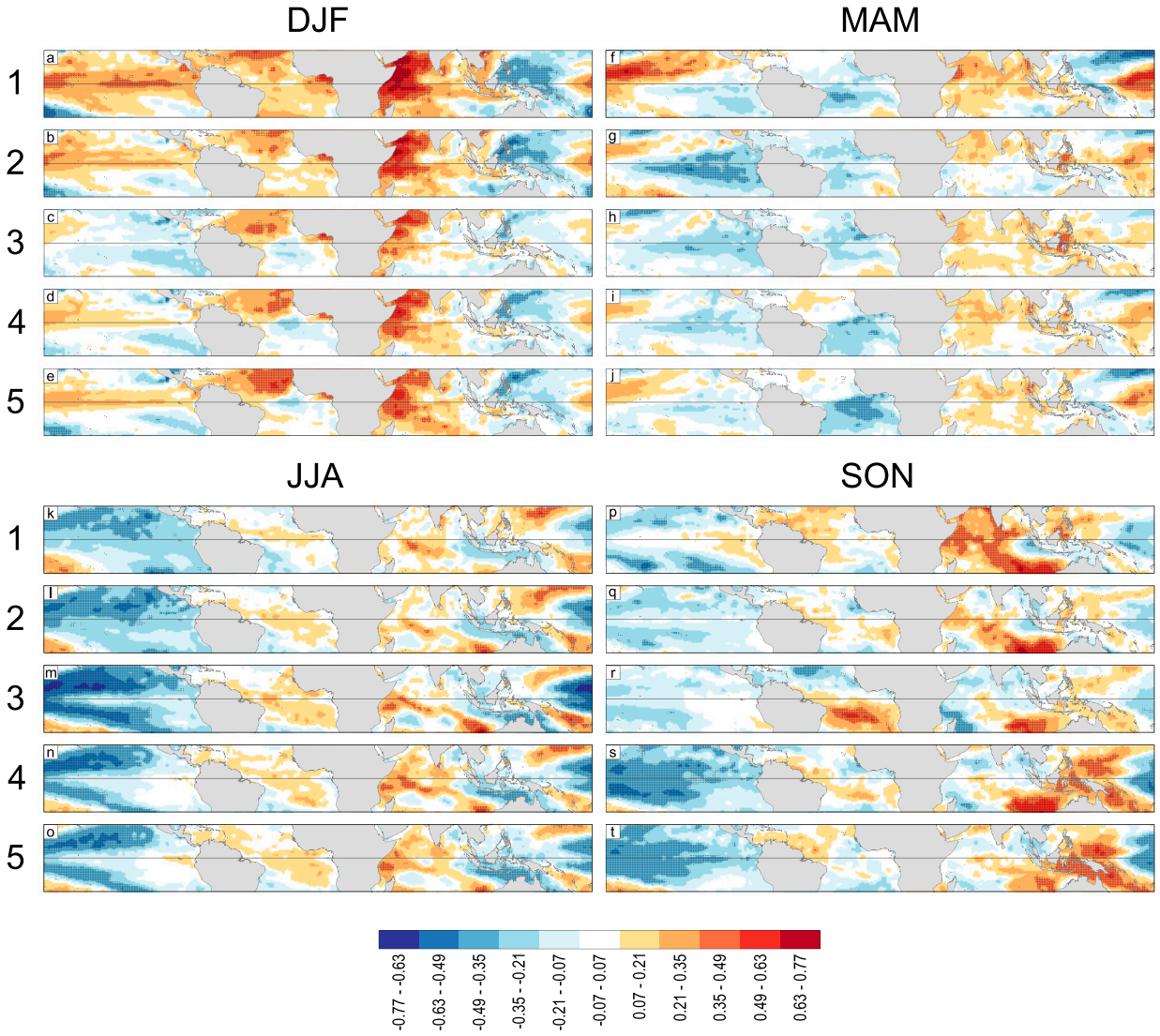

FIG. 4. SST correlations for the five rainfall regions of western Uganda for (a)–(e) DJF, (f)–(j) MAM, (k)–(o) JJA, and (p)–(t) SON. Stippling indicates significant ($\alpha = 0.05$; two tailed) correlations between rainfall and SSTs.

February (DJF), March–May (MAM), June–August (JJA), and September–November (SON), respectively. These seasons generally match the seasons used in other rainfall–SST studies across equatorial Africa, thereby enabling a comparison of findings. In addition, DJF and JJA encapsulate dry seasons for much of the region and MAM and SON encapsulate rainy seasons (Fig. 2). All of the time series (i.e., rainfall, SSTs, and indices) were detrended using the trend line from linear regression (e.g., Lyon 2014), and all subsequent analyses were performed using residuals. The detrending removes spurious correlations created by trends (e.g., Bahaga et al. 2015). Correlations were assessed using Pearson product-moment correlation tests ($\alpha = 0.05$; two tailed).

The temporal correlations were used to assess the intra-annual variability in interregional differences in rainfall–SST teleconnections. Absolute differences in correlations were calculated for each month-index combination for 10 pairs of regions. The mean absolute difference was then calculated from the 10 values. The mean absolute differences were then found for the Indian Ocean (WTIO, SETIO, and DMI), Pacific Ocean (WP, Niño-4, Niño-3.4, Niño-3, Niño-1+2, and SOI), and Atlantic Ocean (NAT, SAT, and TAMG).

4. Results

a. Seasonal teleconnections with Indian Ocean SSTs

Increased DJF rainfall in all regions was associated with high SSTs across the Indian Ocean, especially the western portion (Figs. 4a–e and 5). All regions had significant positive correlations with SSTs in the western Indian Ocean, and all but regions 3 and 4 had significant correlations with the WTIO index.

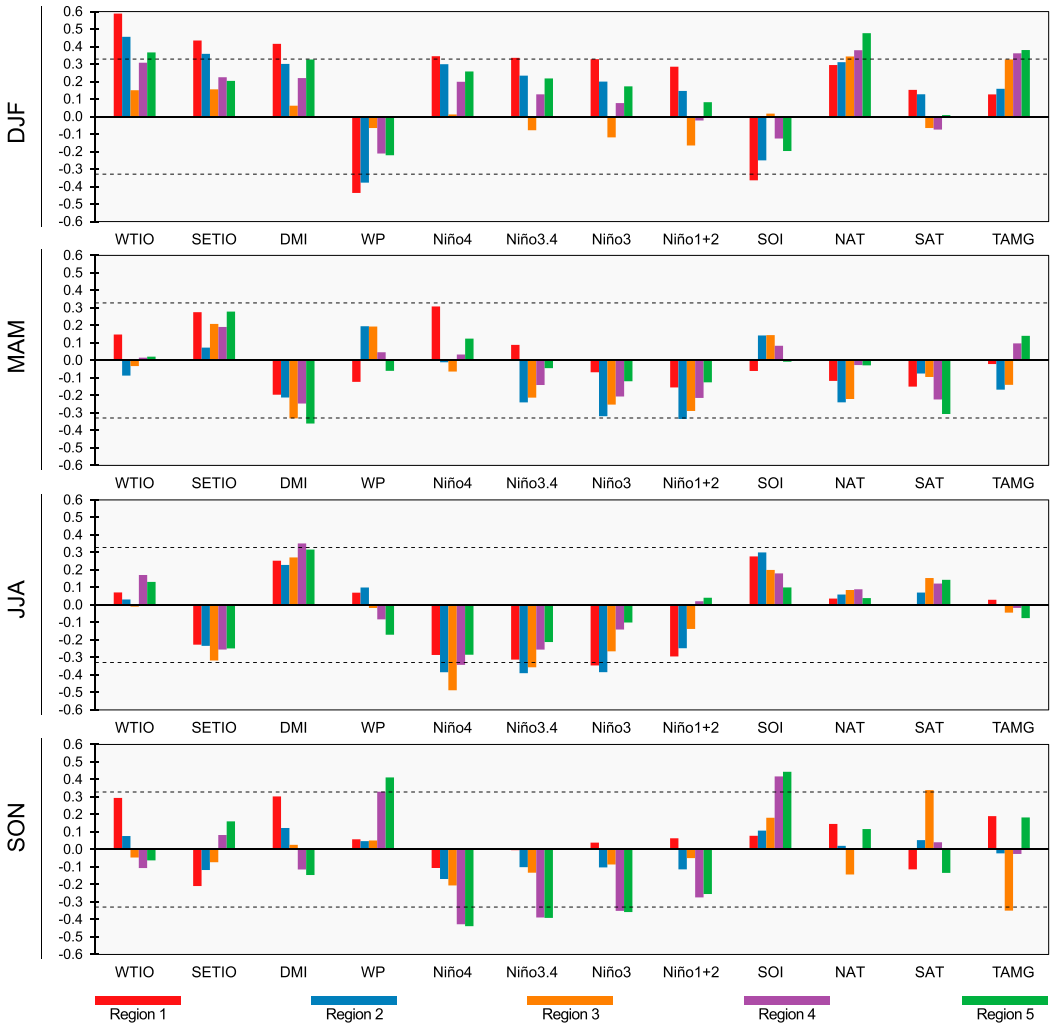

FIG. 5. Correlations between regional rainfall and the 12 indices for the four climatological seasons. Bars extending beyond the dashed lines indicate significant ($\alpha = 0.05$; one tailed) correlations. The indices are described in section 3.

Regions 1 and 2 also had significant positive correlations with the SETIO index. Regions 1 and 5 had significant positive correlations with the DMI.

Increased MAM rainfall in all regions was associated with high SSTs across the Indian Ocean, but the correlations were much weaker than those during DJF (Figs. 4f–j and 5b). None of the regions had rainfall significantly correlated with the WTIO and SETIO indices; however, regions 3 and 5 did have significant negative correlations with the DMI.

The pIOD-like patterns were associated with increased rainfall in western Uganda during boreal summer (Figs. 4k–o and 5d). All regions had significant positive correlations in parts of the western tropical Indian Ocean and all regions, but region 1 had significant negative correlations in parts of the southeastern tropical Indian Ocean. However, only region 4 had a significant positive correlation with the DMI.

Increased SON rainfall in all regions was strongly associated with SSTs across the Indian Ocean, with a pIOD-like pattern linked to region 1 (Figs. 4p–t and 5d). Apart from region 1, none of the regions had strong correlations with the Indian Ocean indices. While region 1 did have strong positive correlations with the WTIO index and the DMI and a strong negative correlation with the SETIO index, none of the correlations were significant. All regions had significant positive correlations with SSTs in the far southeastern Indian Ocean (i.e., south of the SETIO index region). Region 3 had significant negative correlations with SSTs in the southwestern tropical Indian Ocean.

b. Seasonal teleconnections with Pacific Ocean SSTs

Increased DJF rainfall for all regions except region 3, the westernmost region, was associated with El Niño–like SST patterns, but region 1 was the only region with significant correlations (Figs. 4a–e and 5a). While all regions had negative correlations with SSTs in the western tropical Pacific Ocean, only regions 1 and 2 had significant correlations with the WP

index. Region 1 also was the only region with significant positive correlations with any of the Niño indices and an associated significant negative correlation with the SOI.

MAM rainfall was generally weakly correlated with western Pacific Ocean SSTs, with most regions having increased rainfall associated with weak La Niña–like SST patterns (Figs. 4f–j and 5b). Region 1 had significant positive correlations with SSTs in the Niño-4 region, but the correlation with the Niño-4 index was not significant. While most of the regions had strong negative correlative correlations with SSTs in the eastern tropical Pacific Ocean, only region 2 had a significant negative correlation with an associated Niño index.

JJA rainfall for all regions was negatively correlated with central Pacific Ocean SSTs for all regions (Figs. 4k–o and 5d). Only regions 1–3 had significant correlations with at least one Niño index. Regions 1 and 2 also had strong—but not significant—positive correlations with the SOI.

Only the two southernmost regions had strong correlations between SON rainfall and Pacific Ocean SSTs, and increased rainfall in those two regions was associated with La Niña–like SST patterns (Figs. 4p–t and 5d). Regions 4 and 5 had significant negative correlations with central Pacific Ocean SSTs, and thus the Niño-4, Niño-3.4, and Niño-3 indices along with the SOI, and significant positive correlations with the western Pacific Ocean SSTs and the associated WP index. Regions 1–3 had weak correlations with SSTs and the indices.

c. *Teleconnections with Atlantic Ocean SSTs*

DJF rainfall in all regions was positively associated with SSTs in the North Atlantic Ocean and the Gulf of Guinea (Figs. 4a–e and 5a). All regions had strong correlations with the NAT index, but only regions 3–5 had significant positive correlations. These three regions also had significant positive correlations with the TAMG index.

In contrast to the situation for DJF, there were mostly weak teleconnections between regional rainfall and Atlantic Ocean SSTs for the other seasons (Figs. 4k–t and 5b–d). During MAM, significant negative correlations existed across the ocean, particularly in the southern portion (Figs. 4k–o and 5b). However, none of the correlations with the indices were significant (Fig. 5b). There were mostly positive correlations between rainfall and SSTs during JJA, but none of the SST or index correlations were significant. Except for region 3 during SON, there were no significant correlations between rainfall and indices (Fig. 5d). Region 3 had a significant negative correlation with SSTs in the South Atlantic Ocean and significant positive correlations with SSTs in the North Atlantic Ocean, and by extension there were significant negative and positive correlations with the SAT and TAMG indices, respectively (Figs. 4p–t and 5d).

d. *Intra-annual variability in spatial complexity of teleconnections*

Differences among the regions in teleconnections were maximized in October and in general largest during September–December (Figs. 6 and 7). The October peak in differences for the Indian Ocean was the largest of all the differences: the October mean absolute difference in correlations was twice as large as that for the month with second-largest difference. The differences for the Pacific Ocean generally increased from January to October.

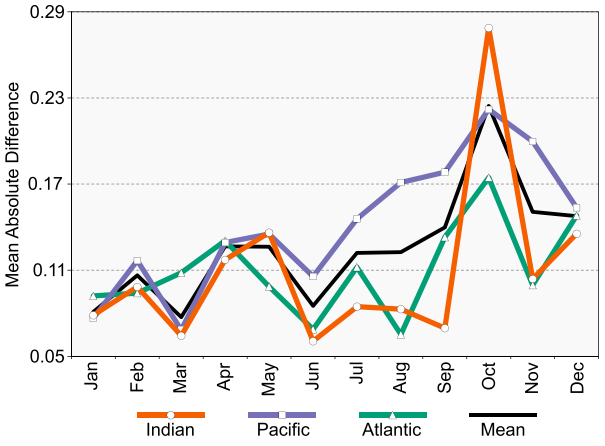

FIG. 6. Intra-annual variations in mean absolute differences in SST correlations among the five rainfall regions. The values for each ocean basin are the mean of the absolute differences in correlation coefficients for each index for each pair of rainfall regions.

There were substantial shifts in teleconnections during September–December (i.e., the period with the largest differences in teleconnections among the regions) (Figs. 7 and 8). September rainfall, especially for regions 1 and 2, was positively correlated with La Niña–like SST patterns (Figs. 8a,b). These patterns also prevailed in July and August, especially for the northern regions (Fig. 7). The teleconnections in regions 1 and 2 were transitioning in October: those regions had rainfall positively correlated with pIOD-like patterns and weak El Niño–like patterns (Figs. 8f,g). The southern regions had nearly the opposite teleconnections (Figs. 8h–j). In November and December, rainfall in regions 1 and 2 was positively correlated with both an El Niño–like SST pattern and a pIOD-like SST pattern (Figs. 8k,l,p,q). The southern regions had much weaker versions of those teleconnections.

5. Discussion

a. *Boreal winter teleconnections*

SSTs in all three tropical oceans are teleconnected to boreal winter rainfall in western Uganda. A warm western Indian Ocean and, to a lesser degree, a pIOD-like pattern are associated with increased rainfall in all regions, and this also has been found for rainfall over all of CEA (Creese and Washington 2016). El Niño–like patterns were positively correlated with rainfall in the northern regions of western Uganda, but these patterns are limited to December and are thus not representative of the entire season. Nevertheless, it is wetter over EEA during El Niño years (de Oliveira et al. 2018); therefore, region 1 during DJF appears to be an extension of EEA. Rainfall in region 3, which is 175 km to the west of region 1 and is essentially in the eastern Congo basin, does not

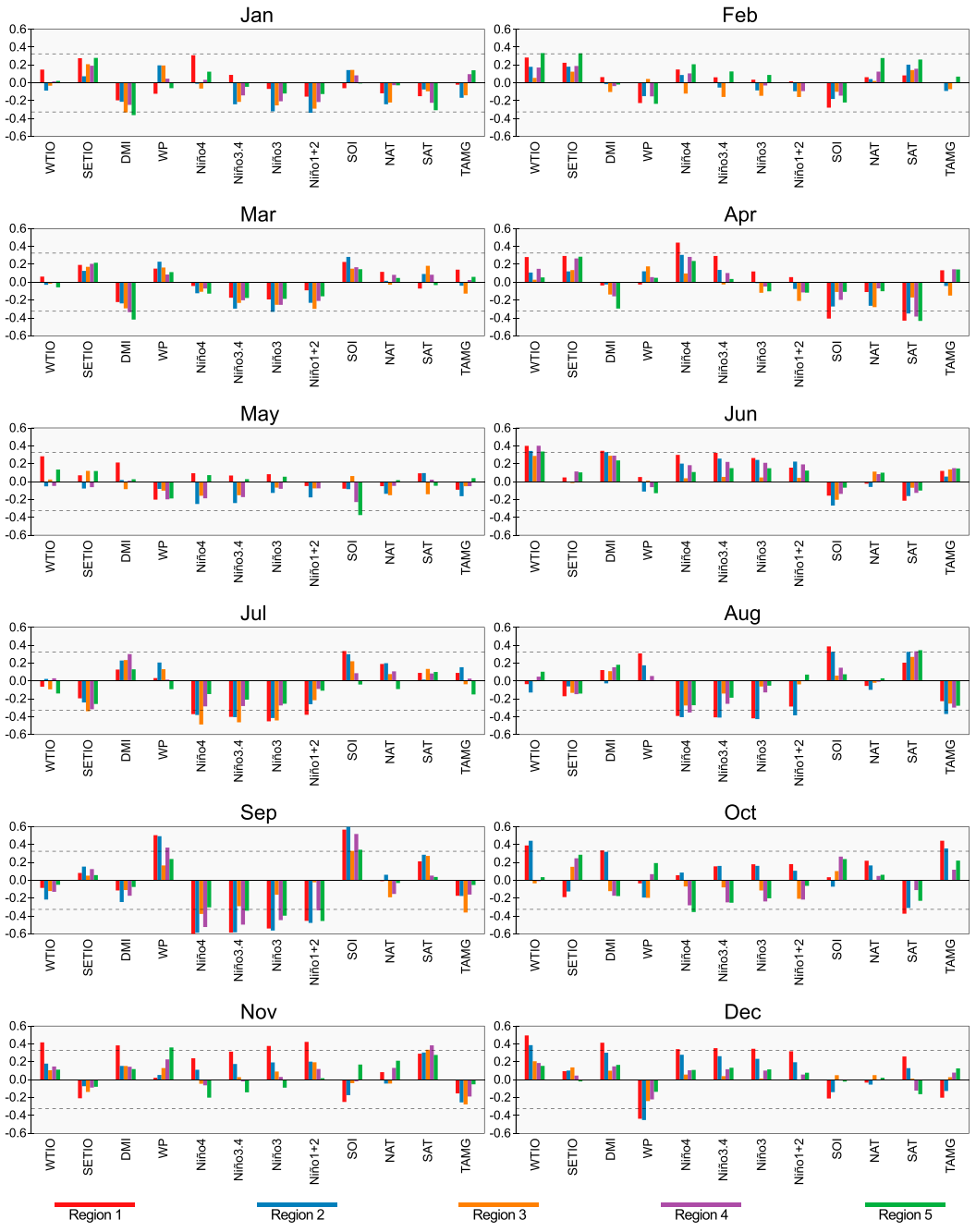

FIG. 7. Correlations between regional rainfall and the 12 indices for each month. Bars extending beyond the dashed lines indicate significant ($\alpha = 0.05$; two tailed) correlations. The indices are described in section 3.

have any connection with El Niño–like patterns. The lack of a teleconnection with ENSO in the eastern Congo basin is expected, since decreased rainfall on the western side of the basin is associated with El Niño–like patterns (Nicholson and Kim 1997; Camberlin et al. 2001). The southern regions (e.g., regions 4 and 5) also have increased rainfall associated with a warm (cool) northern (southern) tropical Atlantic Ocean. The tropical Atlantic Ocean also is a control of CEA rainfall, with the negative SST anomalies in the southern tropical Atlantic Ocean presumed to keep the rain belt near the equator (Balas et al. 2007).

b. *Boreal spring teleconnections*

Among the seasons, boreal spring has the weakest teleconnections between rainfall in western Uganda and tropical SSTs. Western Uganda seems to be more similar to the eastern Congo than EEA during boreal spring: the eastern Congo basin also has rainfall positively correlated with SSTs in the

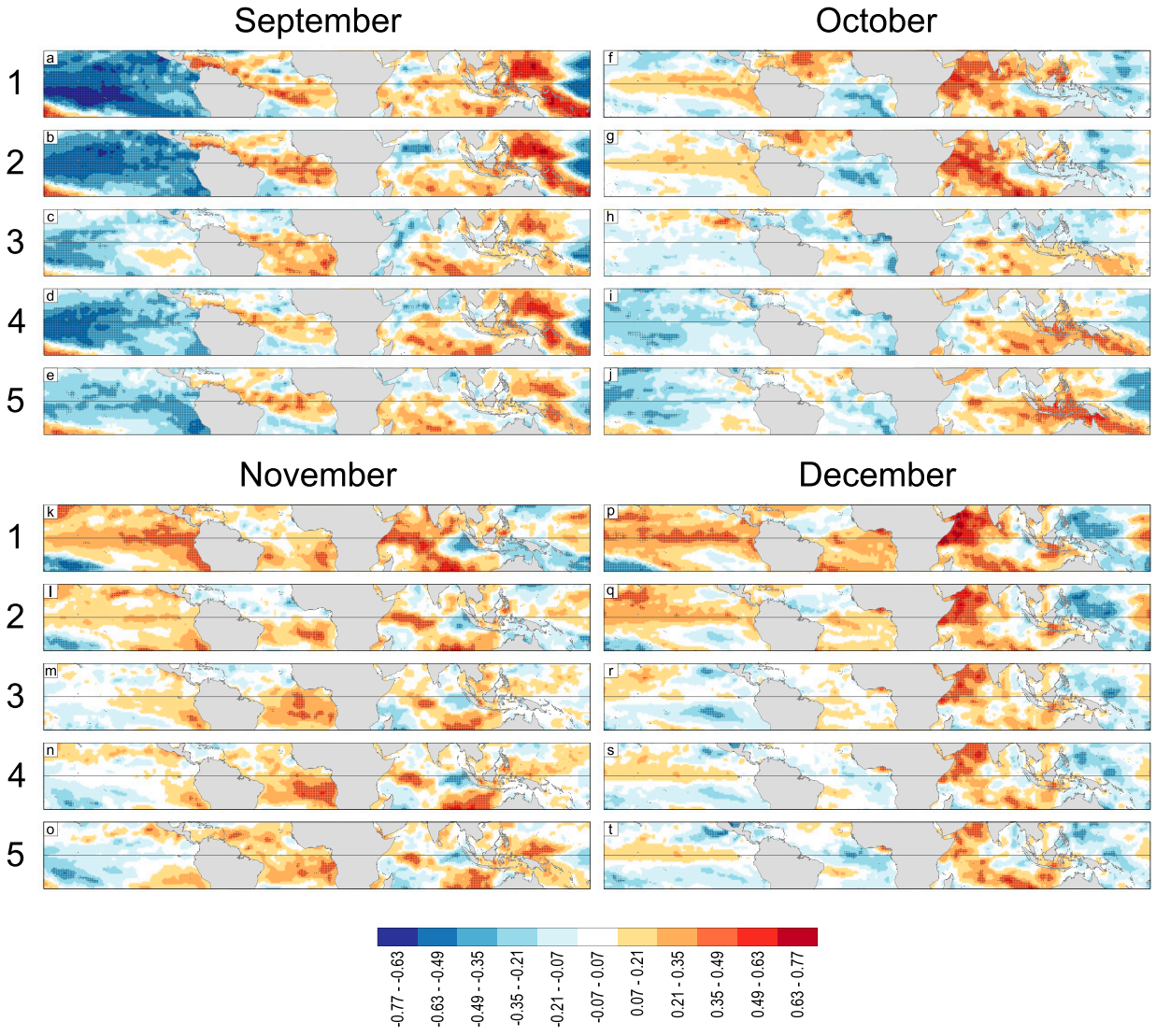

FIG. 8. SST correlations for the five rainfall regions of western Uganda for (a)–(e) September, (f)–(j) October, (k)–(o) November, and (p)–(t) December. Stippling indicates significant ($\alpha = 0.05$; two tailed) correlations between rainfall and SSTs.

western Indian Ocean or a pIOD-like SST pattern (Nicholson and Dezfuli 2013), while for EEA there are weak correlations and mixed results (Omondi et al. 2013; Lyon 2014; Vellinga and Milton 2018). There does not appear to be a clear La Niña–like or El Niño–like pattern associated with increased rainfall in EEA (Camberlin et al. 2001; Camberlin and Philippon 2002; Endris et al. 2019; Lyon 2014), but CEA is similar to western Uganda in that La Niña–like patterns are positively correlated with rainfall (Camberlin et al. 2001; Nicholson and Dezfuli 2013). Western Uganda is like EEA in that it has weak correlations with tropical Atlantic Ocean SSTs, while there are stronger correlations in CEA (Nicholson and Dezfuli 2013).

c. *Boreal summer teleconnections*

The pIOD-like SST patterns, La Niña–like SST patterns, and an anomalously warm southern Atlantic Ocean are teleconnected to increased rainfall in western Uganda during boreal summer. If the months constituting this season are July–September rather than June–August, then the La Niña teleconnection becomes much stronger. The pIOD-like pattern is important for all regions, while the La Niña pattern is more important for the northern regions. EEA generally also has the pIOD-like pattern (Dubache et al. 2019) and a La Niña–like pattern (Camberlin et al. 2001; Segele et al. 2009; Lyon 2014; Gleixner et al. 2017; de Oliveira et al. 2018; Endris et al. 2019) associated with more rainfall. CEA rainfall as a whole is not associated with IOD-like patterns, but—similar to western Uganda and EEA—rainfall in CEA is positively correlated with La Niña–like patterns (Creese and Washington 2016). Rainfall in August and September is correlated with southern Atlantic Ocean SSTs, and a warmer southern Atlantic Ocean should keep the rain belt closer to the equator during boreal summer (Balas et al. 2007).

d. Boreal autumn teleconnections

Boreal autumn has the most spatially complex teleconnections across western Uganda, with the northern regions similar to EEA and the southern regions similar to CEA. While for region 1—and to a lesser degree region 2—rainfall is positively correlated with both pIOD-like and El Niño–like SST patterns for September–November and October–December, the teleconnections are stronger for the latter group of months. The strongest teleconnections are in November and December. El Niño–like or pIOD-like patterns or both also lead to increased rainfall in EEA (Mutai and Ward 2000; Camberlin et al. 2001; Black et al. 2003; Schreck and Semazzi 2004; Behera et al. 2005; Lyon 2014; Bahaga et al. 2015; Wenhaji Ndomeni et al. 2018; Endris et al. 2019). The southern regions do have rainfall positively correlated with Indian Ocean SSTs (but not a pIOD-like pattern). The same relationship with Indian Ocean SSTs has been found for CEA (Dezfuli and Nicholson 2013). Only when September is included as part of boreal autumn does the rest of western Uganda have strong correlations between rainfall and Pacific Ocean SSTs. Rainfall is teleconnected to a La Niña-SST pattern. Neither during September–November, October–December, nor any of the months individually do the southern regions have significant correlations between rainfall and El Niño–like SST patterns. This finding is similar to what was found for CEA in Endris et al. (2019), but it contrasts with results in Dezfuli and Nicholson (2013) showing a strong positive correlation between rainfall in far eastern CEA and El Niño–like SST patterns. The contrast may be due to the much larger latitudinal extent (i.e., 15°) of the region in Dezfuli and Nicholson (2013). While rainfall in western Uganda is positively correlated with northern tropical Atlantic Ocean SSTs and negatively correlated with southern Atlantic Ocean SSTs, the lack of research on Atlantic Ocean teleconnections and rainfall in EEA and CEA makes it difficult to contextualize these findings.

6. Conclusions

There is considerable intra-annual and interregional variability in rainfall–SST teleconnections for western Uganda, which has traditionally been considered to have rainfall totals and seasonal rainfall variability that are transitional between EEA and CEA. Based on teleconnections, northwestern Uganda and southwestern Uganda are more similar to EEA and CEA, respectively. Rainfall throughout western Uganda is teleconnected to SSTs in all tropical oceans, but much more so to SSTs in the Indian and Pacific Oceans than the Atlantic Ocean. Increased Indian Ocean SSTs during boreal winter, spring, and autumn and a pIOD-like pattern during boreal summer are associated with increased rainfall throughout western Uganda, and this is generally true for both EEA and CEA. During boreal autumn and winter, only northwestern Uganda has increased rainfall associated with a pIOD-like pattern or an El Niño–like SST pattern. Southwestern Uganda does not have these teleconnections; therefore, it would be a mistake to assume that either the IOD or ENSO or both have a significant impact on rainfall there during September–December. In fact, Atlantic Ocean SSTs, which might be overlooked by seasonal forecasters in the region, appear to impact rainfall in southwestern Uganda in boreal winter and summer, which aligns with what has been found for CEA. Future studies should extend this work over a much larger geographic scale (e.g., all of equatorial Africa) to determine the extent of the rainfall–SST teleconnection zone that includes southwestern Uganda and the spatial gradient in teleconnections that exist across the Congo basin, which has been much less studied than East Africa.

Acknowledgments. This research was supported by the National Science Foundation (Award 1740201) and approved by the Uganda National Council for Science and Technology.

Data availability statement. All gridded rainfall data, SST data, and indices data used in this study are publicly available. CHIRPS and TAMSAT, the gridded rainfall products, were obtained from the International Research Institute for Climate and Society (https://iridl.ldeo.columbia.edu/). OISSTV2 data (i.e., gridded SST data) were obtained from the National Oceanic and Atmospheric Administration (https://psl.noaa.gov/data/gridded/data.noaa.oisst.v2.highres.html). All SST indices and the SOI data were obtained from NOAA (https://stateoftheocean.osmc.noaa.gov). Daily rainfall data for the rainfall regions in this paper—as well as geospatial data for the regions—can be accessed online (https://data.mendeley.com/datasets/ppxktx233y/2).

REFERENCES

Bahaga, T. K., G. Mengistu Tsidu, F. Kucharski, and G. T. Diro, 2015: Potential predictability of the sea-surface temperature forced equatorial East African short rains interannual variability in the 20th century. *Quart. J. Roy. Meteor. Soc.*, **141**, 16–26, https://doi.org/10.1002/qj.2338.

Balas, N., S. E. Nicholson, and D. Klotter, 2007: The relationship of rainfall variability in west central Africa to sea-surface temperature fluctuations. *Int. J. Climatol.*, **27**, 1335–1349, https://doi.org/10.1002/joc.1456.

Behera, S. K., J.-J. Luo, S. Masson, P. Delecluse, S. Gualdi, A. Navarra, and T. Yamagata, 2005: Paramount impact of the Indian Ocean dipole on the East African short rains: A CGCM study. *J. Climate*, **18**, 4514–4530, https://doi.org/10.1175/JCLI3541.1.

Berhane, F., B. Zaitchik, and A. Dezfuli, 2014: Subseasonal analysis of precipitation variability in the Blue Nile River basin. *J. Climate*, **27**, 325–344, https://doi.org/10.1175/JCLI-D-13-00094.1.

Black, E., 2005: The relationship between Indian Ocean sea-surface temperature and East African rainfall. *Philos. Trans. Roy. Soc.*, **363A**, 43–47, https://doi.org/10.1098/rsta.2004.1474.

——, J. Slingo, and K. R. Sperber, 2003: An observational study of the relationship between excessively strong short rains in coastal East Africa and Indian Ocean SST. *Mon. Wea. Rev.*, **131**, 74–94, https://doi.org/10.1175/1520-0493(2003)131<0074:AOSOTR>2.0.CO;2.

Camberlin, P., and N. Philippon, 2002: The East African March–May rainy season: Associated atmospheric dynamics and

predictability over the 1968–97 period. *J. Climate*, **15**, 1002–1019, https://doi.org/10.1175/1520-0442(2002)015<1002:TEAMMR>2.0.CO;2.

——, S. Janicot, and I. Poccard, 2001: Seasonality and atmospheric dynamics of the teleconnection between African rainfall and tropical sea-surface temperature: Atlantic vs. ENSO. *Int. J. Climatol.*, **21**, 973–1005, https://doi.org/10.1002/joc.673.

——, V. Moron, R. Okoola, N. Philippon, and W. Gitau, 2009: Components of rainy seasons' variability in equatorial East Africa: Onset, cessation, rainfall frequency and intensity. *Theor. Appl. Climatol.*, **98**, 237–249, https://doi.org/10.1007/s00704-009-0113-1.

Chang, P., L. Ji, and H. Li, 1997: A decadal climate variation in the tropical Atlantic Ocean from thermodynamic air-sea interactions. *Nature*, **385**, 516–518, https://doi.org/10.1038/385516a0.

Cook, K. H., and E. K. Vizy, 2016: The Congo basin Walker circulation: Dynamics and connections to precipitation. *Climate Dyn.*, **47**, 697–717, https://doi.org/10.1007/s00382-015-2864-y.

Cooper, P. J. M., J. Dimes, K. P. C. Rao, B. Shapiro, B. Shiferaw, and S. Twomlow, 2008: Coping better with current climatic variability in the rain-fed farming systems of sub-Saharan Africa: An essential first step in adapting to future climate change? *Agric. Ecosyst. Environ.*, **126**, 24–35, https://doi.org/10.1016/j.agee.2008.01.007.

Costa, K., J. Russell, B. Konecky, and H. Lamb, 2014: Isotopic reconstruction of the African Humid Period and Congo Air Boundary migration at Lake Tana, Ethiopia. *Quat. Sci. Rev.*, **83**, 58–67, https://doi.org/10.1016/j.quascirev.2013.10.031.

Crane, T. A., C. Roncoli, and G. Hoogenboom, 2011: Adaptation to climate change and climate variability: The importance of understanding agriculture as performance. *NJAS Wageningen J. Life Sci.*, **57**, 179–185, https://doi.org/10.1016/j.njas.2010.11.002.

Creese, A., and R. Washington, 2016: Using qflux to constrain modeled Congo basin rainfall in the CMIP5 ensemble. *J. Geophys. Res. Atmos.*, **121**, 13 415–13 442, https://doi.org/10.1002/2016JD025596.

——, and ——, 2018: A process-based assessment of CMIP5 rainfall in the Congo basin: The September–November rainy season. *J. Climate*, **31**, 7417–7439, https://doi.org/10.1175/JCLI-D-17-0818.1.

Degefu, M. A., D. P. Rowell, and W. Bewket, 2017: Teleconnections between Ethiopian rainfall variability and global SSTs: Observations and methods for model evaluation. *Meteor. Atmos. Phys.*, **129**, 173–186, https://doi.org/10.1007/s00703-016-0466-9.

de Oliveira, C. P., L. Aímola, T. Ambrizzi, and A. C. V. Freitas, 2018: The Influence of the regional Hadley and Walker circulations on precipitation patterns over Africa in El Niño, La Niña, and neutral years. *Pure Appl. Geophys.*, **175**, 2293–2306, https://doi.org/10.1007/s00024-018-1782-4.

Dezfuli, A., 2017: Climate of western and central equatorial Africa. *Oxford Research Encyclopedia of Climate Science*, Oxford University Press, https://doi.org/10.1093/acrefore/9780190228620.013.511.

——, and S. E. Nicholson, 2013: The relationship of rainfall variability in western equatorial Africa to the tropical oceans and atmospheric circulation. Part II: The boreal autumn. *J. Climate*, **26**, 66–84, https://doi.org/10.1175/JCLI-D-11-00686.1.

Diem, J. E., J. Hartter, J. Salerno, E. McIntyre, and A. Stuart Grandy, 2017: Comparison of measured multi-decadal rainfall variability with farmers' perceptions of and responses to seasonal changes in western Uganda. *Reg. Environ. Change*, **17**, 1127–1140, https://doi.org/10.1007/s10113-016-0943-1.

——, B. L. Konecky, J. Salerno, and J. Hartter, 2019a: Is equatorial Africa getting wetter or drier? Insights from an evaluation of long-term, satellite-based rainfall estimates for western Uganda. *Int. J. Climatol.*, **39**, 3334–3347, https://doi.org/10.1002/joc.6023.

——, H. S. Sung, B. L. Konecky, M. W. Palace, J. Salerno, and J. Hartter, 2019b: Rainfall characteristics and trends—and the role of Congo westerlies—in the western Uganda transition zone of equatorial Africa from 1983 to 2017. *J. Geophys. Res. Atmos.*, **124**, 10 712–10 729, https://doi.org/10.1029/2019JD031243.

Dubache, G., B. A. Ogwang, V. Ongoma, and A. R. M. Towfiqul Islam, 2019: The effect of Indian Ocean on Ethiopian seasonal rainfall. *Meteor. Atmos. Phys.*, **131**, 1753–1761, https://doi.org/10.1007/s00703-019-00667-8.

Endris, H. S., C. Lennard, B. Hewitson, A. Dosio, G. Nikulin, and G. A. Artan, 2019: Future changes in rainfall associated with ENSO, IOD and changes in the mean state over eastern Africa. *Climate Dyn.*, **52**, 2029–2053, https://doi.org/10.1007/s00382-018-4239-7.

Farrow, A., D. Musoni, S. Cook, and R. Buruchara, 2011: Assessing the risk of root rots in common beans in East Africa using simulated, estimated and observed daily rainfall data. *Exp. Agric.*, **47**, 357–373, https://doi.org/10.1017/S0014479710000980.

Funk, C., and Coauthors, 2015: The climate hazards infrared precipitation with stations—A new environmental record for monitoring extremes. *Sci. Data*, **2**, 150066, https://doi.org/10.1038/sdata.2015.66.

Gleixner, S., N. Keenlyside, E. Viste, and D. Korecha, 2017: The El Niño effect on Ethiopian summer rainfall. *Climate Dyn.*, **49**, 1865–1883, https://doi.org/10.1007/s00382-016-3421-z.

Hartter, J., M. D. Stampone, S. J. Ryan, K. Kirner, C. A. Chapman, and A. Goldman, 2012: Patterns and perceptions of climate change in a biodiversity conservation hotspot. *PLOS ONE*, **7**, e32408, https://doi.org/10.1371/journal.pone.0032408.

Hastenrath, S., and D. Polzin, 2004: Dynamics of the surface wind field over the equatorial Indian Ocean. *Quart. J. Roy. Meteor. Soc.*, **130**, 503–517, https://doi.org/10.1256/qj.03.79.

Herrmann, S. M., and K. I. Mohr, 2011: A continental-scale classification of rainfall seasonality regimes in Africa based on gridded precipitation and land surface temperature products. *J. Appl. Meteor. Climatol.*, **50**, 2504–2513, https://doi.org/10.1175/JAMC-D-11-024.1.

Hoell, A., and C. Funk, 2013: The ENSO-related west Pacific sea surface temperature gradient. *J. Climate*, **26**, 9545–9562, https://doi.org/10.1175/JCLI-D-12-00344.1.

King, J. A., R. Washington, and S. Engelstaedter, 2020: Representation of the Indian Ocean Walker circulation in climate models and links to Kenyan rainfall. *Int. J. Climatol.*, **41** (Suppl. S1), E616–E643, https://doi.org/10.1002/joc.6714.

Lau, K.-M., and S. Yang, 2015: Walker circulation. *Encyclopedia of Atmospheric Sciences*, G. R. North, J. Pyle, and F. Zhang, Eds., Elsevier, 177–181.

Levin, N. E., E. J. Zipser, and T. E. Cerling, 2009: Isotopic composition of waters from Ethiopia and Kenya: Insights into moisture sources for eastern Africa. *J. Geophys. Res.*, **114**, D23306, https://doi.org/10.1029/2009JD012166.

Liebmann, B., I. Bladé, G. N. Kiladis, L. M. V. Carvalho, G. B. Senay, D. Allured, S. Leroux, and C. Funk, 2012: Seasonality

of African precipitation from 1996 to 2009. *J. Climate*, **25**, 4304–4322, https://doi.org/10.1175/JCLI-D-11-00157.1.

——, and Coauthors, 2014: Understanding recent eastern Horn of Africa rainfall variability and change. *J. Climate*, **27**, 8630–8645, https://doi.org/10.1175/JCLI-D-13-00714.1.

Lyon, B., 2014: Seasonal drought in the Greater Horn of Africa and its recent increase during the March–May long rains. *J. Climate*, **27**, 7953–7975, https://doi.org/10.1175/JCLI-D-13-00459.1.

MacLeod, D., R. Graham, C. O'Reilly, G. Otieno, and M. Todd, 2021: Causal pathways linking different flavours of ENSO with the Greater Horn of Africa short rains. *Atmos. Sci. Lett.*, **22**, e1015, https://doi.org/10.1002/asl.1015.

Maidment, R. I., and Coauthors, 2017: A new, long-term daily satellite-based rainfall dataset for operational monitoring in Africa. *Sci. Data*, **4**, 170063, http://doi.org/10.1038/sdata.2017.63.

Marshall, J., A. Donohoe, D. Ferreira, and D. McGee, 2014: The ocean's role in setting the mean position of the inter-tropical convergence zone. *Climate Dyn.*, **42**, 1967–1979, https://doi.org/10.1007/s00382-013-1767-z.

Mélice, J.-L., and J. Servain, 2003: The tropical Atlantic meridional SST gradient index and its relationships with the SOI, NAO and Southern Ocean. *Climate Dyn.*, **20**, 447–464, https://doi.org/10.1007/s00382-002-0289-x.

Monaghan, A. J., K. MacMillan, S. M. Moore, P. S. Mead, M. H. Hayden, and R. J. Eisen, 2012: A regional climatography of West Nile, Uganda, to support human plague modeling. *J. Appl. Meteor. Climatol.*, **51**, 1201–1221, https://doi.org/10.1175/JAMC-D-11-0195.1.

Mutai, C. C., and M. N. Ward, 2000: East African rainfall and the tropical circulation/convection on intraseasonal to interannual timescales. *J. Climate*, **13**, 3915–3939, https://doi.org/10.1175/1520-0442(2000)013<3915:EARATT>2.0.CO;2.

Ngecu, W. M., and E. M. Mathu, 1999: The El-Nino-triggered landslides and their socioeconomic impact on Kenya. *Environ. Geol.*, **38**, 277–284, https://doi.org/10.1007/s002540050425.

Nicholson, S. E., 2000: The nature of rainfall variability over Africa on time scales of decades to millenia. *Global Planet. Change*, **26**, 137–158, https://doi.org/10.1016/S0921-8181(00)00040-0.

——, 2014: A detailed look at the recent drought situation in the Greater Horn of Africa. *J. Arid Environ.*, **103**, 71–79, https://doi.org/10.1016/j.jaridenv.2013.12.003.

——, 2015: Long-term variability of the East African 'short rains' and its links to large-scale factors. *Int. J. Climatol.*, **35**, 3979–3990, https://doi.org/10.1002/joc.4259.

——, 2017: Climate and climatic variability of rainfall over eastern Africa. *Rev. Geophys.*, **55**, 590–635, https://doi.org/10.1002/2016RG000544.

——, 2018: The ITCZ and the seasonal cycle over equatorial Africa. *Bull. Amer. Meteor. Soc.*, **99**, 337–348, https://doi.org/10.1175/BAMS-D-16-0287.1.

——, and J. Kim, 1997: The relationship of the El Niño–Southern Oscillation to African rainfall. *Int. J. Climatol.*, **17**, 117–135, https://doi.org/10.1002/(SICI)1097-0088(199702)17:2<117::AID-JOC84>3.0.CO;2-O.

——, and A. K. Dezfuli, 2013: The relationship of rainfall variability in western equatorial Africa to the tropical oceans and atmospheric circulation. Part I: The boreal spring. *J. Climate*, **26**, 45–65, https://doi.org/10.1175/JCLI-D-11-00653.1.

Okonya, J. S., K. Syndikus, and J. Kroschel, 2013: Farmers' perception of and coping strategies to climate change: Evidence from six agro-ecological zones of Uganda. *J. Agric. Sci.*, **5**, 252–263, https://doi.org/10.5539/jas.v5n8p252.

Omondi, P., L. A. Ogallo, R. Anyah, J. M. Muthama, and J. Ininda, 2013: Linkages between global sea surface temperatures and decadal rainfall variability over eastern Africa region. *Int. J. Climatol.*, **33**, 2082–2104, https://doi.org/10.1002/joc.3578.

Osbahr, H., P. Dorward, R. Stern, and S. Cooper, 2011: Supporting agricultural innovation in Uganda to respond to climate risk: Linking climate change and variability with farmer perceptions. *Exp. Agric.*, **47**, 293–316, https://doi.org/10.1017/S0014479710000785.

Reynolds, R. W., N. A. Rayner, T. M. Smith, D. C. Stokes, and W. Wang, 2002: An improved in situ and satellite SST analysis for climate. *J. Climate*, **15**, 1609–1625, https://doi.org/10.1175/1520-0442(2002)015<1609:AIISAS>2.0.CO;2.

Roncoli, C., K. Ingram, and P. Kirshen, 2002: Reading the rains: Local knowledge and rainfall forecasting in Burkina Faso. *Soc. Nat. Resour.*, **15**, 409–427, https://doi.org/10.1080/08941920252866774.

——, B. S. Orlove, M. R. Kabugo, and M. M. Waiswa, 2011: Cultural styles of participation in farmers' discussions of seasonal climate forecasts in Uganda. *Agric. Hum. Values*, **28**, 123–138, https://doi.org/10.1007/s10460-010-9257-y.

Saji, N. H., B. N. Goswami, P. N. Vinayachandran, and T. Yamagata, 1999: A dipole mode in the tropical Indian Ocean. *Nature*, **401**, 360–363, https://doi.org/10.1038/43854.

Salerno, J., J. E. Diem, B. L. Konecky, and J. Hartter, 2019: Recent intensification of the seasonal rainfall cycle in equatorial Africa revealed by farmer perceptions, satellite-based estimates, and ground-based station measurements. *Climatic Change*, **153**, 123–139, https://doi.org/10.1007/s10584-019-02370-4.

Schott, F. A., S.-P. Xie, and J. P. McCreary, 2009: Indian Ocean circulation and climate variability. *Rev. Geophys.*, **47**, RG1002, https://doi.org/10.1029/2007RG000245.

Schreck, C. J., and F. H. M. Semazzi, 2004: Variability of the recent climate of eastern Africa. *Int. J. Climatol.*, **24**, 681–701, https://doi.org/10.1002/joc.1019.

Segele, Z. T., P. J. Lamb, and L. M. Leslie, 2009: Seasonal-to-interannual variability of Ethiopia/Horn of Africa monsoon. Part I: Associations of wavelet-filtered large-scale atmospheric circulation and global sea surface temperature. *J. Climate*, **22**, 3396–3421, https://doi.org/10.1175/2008JCLI2859.1.

Ssempiira, J., J. Kissa, B. Nambuusi, E. Mukooyo, J. Opigo, F. Makumbi, S. Kasasa, and P. Vounatsou, 2018: Interactions between climatic changes and intervention effects on malaria spatio-temporal dynamics in Uganda. *Parasite Epidemiol. Control*, **3**, e00070, https://doi.org/10.1016/j.parepi.2018.e00070.

Todd, M. C., and R. Washington, 2004: Climate variability in central equatorial Africa: Influence from the Atlantic sector. *Geophys. Res. Lett.*, **31**, L23202, https://doi.org/10.1029/2004GL020975.

UNMA, 2021: Seasonal forecasts. Accessed 19 March 2021, https://www.unma.go.ug/seasonal-forecasts/.

Vellinga, M., and S. F. Milton, 2018: Drivers of interannual variability of the East African "long rains." *Quart. J. Roy. Meteor. Soc.*, **144**, 861–876, https://doi.org/10.1002/qj.3263.

Webster, P. J., 2004: The elementary Hadley circulation. *The Hadley Circulation: Present, Past and Future*, H. F. Diaz and R. S. Bradley, Eds., Springer, 9–60.

Wenhaji Ndomeni, C., E. Cattani, A. Merino, and V. Levizzani, 2018: An observational study of the variability of East African rainfall with respect to sea surface temperature and soil moisture. *Quart. J. Roy. Meteor. Soc.*, **144**, 384–404, https://doi.org/10.1002/qj.3255.

Wilkie, D., G. Morelli, F. Rotberg, and E. Shaw, 1999: Wetter isn't better: Global warming and food security in the Congo basin. *Global Environ. Change*, **9**, 323–328, https://doi.org/10.1016/S0959-3780(99)00021-7.

Zougmoré, R. B., S. T. Partey, M. Ouédraogo, E. Torquebiau, and B. M. Campbell, 2018: Facing climate variability in sub-Saharan Africa: Analysis of climate-smart agriculture opportunities to manage climate-related risks. *Cah. Agric.*, **27**, 34001, https://doi.org/10.1051/cagri/2018019.